

PatchGuard: Adversarially Robust Anomaly Detection and Localization through Vision Transformers and Pseudo Anomalies

Mojtaba Nafez¹ Amirhossein Koochakian¹ * Arad Maleki¹ *
 Jafar Habibi¹ Mohammad Hossein Rohban¹
¹Sharif University of Technology, Iran

{mojtaba.nafez77, amir.koochakian12, arad.maleki02, rohban}@sharif.edu

Abstract

Anomaly Detection (AD) and Anomaly Localization (AL) are crucial in fields that demand high reliability, such as medical imaging and industrial monitoring. However, current AD and AL approaches are often susceptible to adversarial attacks due to limitations in training data, which typically include only normal, unlabeled samples. This study introduces PatchGuard, an adversarially robust AD and AL method that incorporates pseudo anomalies with localization masks within a Vision Transformer (ViT)-based architecture to address these vulnerabilities. We begin by examining the essential properties of pseudo anomalies, and follow it by providing theoretical insights into the attention mechanisms required to enhance the adversarial robustness of AD and AL systems. We then present our approach, which leverages Foreground-Aware Pseudo-Anomalies to overcome the deficiencies of previous anomaly-aware methods. Our method incorporates these crafted pseudo-anomaly samples into a ViT-based framework, with adversarial training guided by a novel loss function designed to improve model robustness, as supported by our theoretical analysis. Experimental results on well-established industrial and medical datasets demonstrate that PatchGuard significantly outperforms previous methods in adversarial settings, achieving performance gains of 53.2% in AD and 68.5% in AL, while also maintaining competitive accuracy in non-adversarial settings. The code repository is available at [here](#).

1. Introduction

In recent years, Anomaly Detection (AD) and Anomaly Localization (AL) have become critical techniques across various fields, including medical imaging, fraud detection, and industrial monitoring [24, 38, 47, 53, 77, 79, 82]. While state-of-the-art (SOTA) AD and AL methods exhibit near-perfect performance on standard benchmarks [7, 94], they

*Equal Contribution

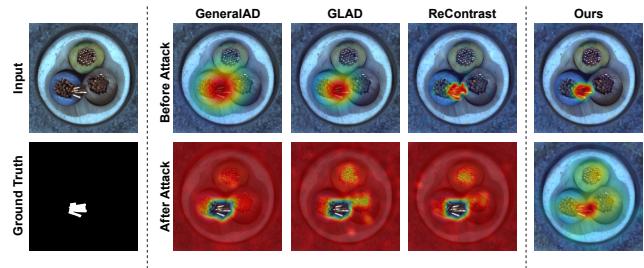


Figure 1. **Impact of Adversarial Attacks on Anomaly Localization Methods:** Localization maps for multiple methods are shown before and after a PGD-1000 attack, illustrating the vulnerability of existing methods to adversarial attacks, even when performing perfectly in clean conditions. Our proposed method demonstrates enhanced robustness in these adversarial scenarios.

frequently face significant performance degradation when subjected to adversarial attacks, as illustrated in Figure 1 [13, 62, 73, 75, 83, 92]. These attacks involve introducing subtle, imperceptible perturbations into the input data, misleading models to misclassify normal¹ samples as anomalies or to overlook actual anomalies [2, 26, 54, 74, 91]. To address this vulnerability, a variety of strategies have been proposed to strengthen the adversarial robustness of AD systems [4, 8, 11, 27, 50, 70]. However, despite these advancements, the resilience of these methods remains limited, with even mild adversarial attacks still causing noticeable performance drops, even on widely used anomaly benchmarks [7, 94]. Furthermore, adversarial robustness in AL remains an unexplored area, highlighting a critical gap in the current research.

Adversarial training, a strategy designed to improve model robustness in classification tasks, incorporates adversarial samples into the training process [54, 85]. Despite its success in standard classification, this approach proves less effective in AD and AL scenarios [57]. The primary obstacle

¹In this study, the term ‘normal’ refers to inlier samples, not to be mistaken with Gaussian distribution.

to achieving adversarial robustness in AD lies in the absence of anomalous samples during training [11, 12]. Without such samples, models cannot be trained on adversarial perturbations specific to anomalous data [6, 57, 64, 67], leaving them vulnerable to attacks on perturbed anomalies [4, 11, 12]. To address this issue in the AD setup, recent efforts have combined Outlier Exposure (OE) [34] with adversarial training [4, 11, 12, 60]. However, this method struggles when applied to high-resolution, real-world datasets [57]. This challenge is even more pronounced in AL settings, as robust AL methods must perform pixel-level classification, which inherently requires pixel-level supervision, while at the same time operating within the same data constraints as the AD framework [37, 93]. Despite ongoing research, the adversarial robustness of AL methods remains an open problem, with no comprehensive solutions proposed to date.

In this study, we identify two essential properties that OE techniques must satisfy for effective application in adversarially robust AD and AL. First, the outlier exposures must include localization maps to facilitate the training of robust AL models. This requirement aligns with prior research on adversarially robust segmentation models, which underscores the importance of generating localization maps to enhance model robustness [43, 52, 78]. Second, as noted by [57], OE samples should be “near-distributed” relative to normal data, meaning they should share similar semantic and stylistic attributes. This condition is consistent with the literature on adversarial robustness, which highlights the advantages of near-distribution decision boundaries samples for optimizing the model robustness [80].

Moreover, the recent success of Vision Transformer (ViT)-based architectures in clean AD and AL tasks [16, 39, 45, 73], attributed to their global contextual modeling [21], motivated us to explore their potential in adversarial settings. For an input image x and a fixed attention layer ℓ , we define the *Attention Degree* of ℓ under x as the average number of input embeddings each output embedding attends to. As shown in Figure 2, we observe that images that induce higher attention degrees in the model are more resistant to adversarial attacks. Furthermore, adversarial training appears to implicitly steer the model toward achieving a high attention degree. We provide a theoretical analysis and justification for these findings in Section 4.

Building on these insights, we propose PatchGuard, an adversarially robust AD and AL method that addresses limitations in current OE-based methods and leverages attention-based insights. To address OE challenges, we generate pseudo-anomaly samples from normal data, ensuring they meet two essential criteria: availability of localization maps and near-distribution alignment with inliers. To create samples that exhibit anomalous characteristics while remaining close to the inlier distribution, we introduce Foreground-Aware Pseudo-Anomaly Generation. This approach iden-

tifies causal regions in normal samples using an enhanced Grad-CAM [69] feature attribution technique with tailored augmentations. These identified regions are then selectively distorted, drawing on insights from [63], to produce anomaly samples that retain stylistic and semantic coherence with the original data. By precisely controlling the distortion location, we can generate accurate localization maps for the pseudo-anomalies, effectively meeting both criteria for robust AD and AL.

In the next step, we leverage normal samples and pseudo-anomalies to perform adversarial training on a ViT-based architecture. Building on the provided insights, we introduce a novel loss function designed to increase the model’s last-layer attention degree. As our theoretical justifications suggest, this property significantly enhances the model’s adversarial robustness in both AD and AL settings.

Contribution. In this paper, we propose PatchGuard, an adversarially robust AD and AL method. To the best of our knowledge, we are the first to raise and effectively address the issue of adversarial robustness in AL. We provide insights into the shortcomings of previous OE-based methods and introduce the Foreground-Aware Pseudo-Anomaly Generation framework to address these limitations. Additionally, we provide insights and theoretical justifications on enhancing the adversarial robustness of ViT-based architectures, and propose a novel loss function aligned with these findings. We evaluate PatchGuard in both clean and adversarial settings, rigorously testing its robustness under several strong attacks, including PGD-1000 [54], A³ [48], and SEA [18]. Results demonstrate that PatchGuard significantly outperforms existing methods in adversarial contexts, achieving an AUROC improvement of 53.2% in AD and 68.5% in AL, while maintaining competitive performance in standard conditions. Our evaluations span various well-established industrial and medical datasets, including MVTEC [7], VisA [94], and BraTS2021 [5], highlighting PatchGuard’s applicability.

2. Related Work

From an adversarial robustness perspective, anomaly detection and localization methods can be mainly classified into three categories: 1) methods with anomaly-free training, 2) methods that leverage anomalies at the embedding level, and 3) methods that leverage anomalies at the input level. We experimentally adapted methods from each category to adversarial training processes, and the results reveal they still exhibit significant vulnerabilities even after adversarial training. The first category consists of methods such as Recontrast[31], Transformaly [16], and PatchCore [66], that operate on the hypothesis that models trained exclusively on normal samples can reconstruct normal images well but fail to do so with abnormal regions. These methods lack robustness, since the model does not encounter any anomaly

data during adversarial training, meaning that when adversarial perturbations are added to anomaly data, the model still remains vulnerable. The second category, which includes methods such as SimpleNet [49], GeneralAD [73], UniAD [84], and DSR [90], utilize a feature extractor during training to obtain feature vectors of the normal set. By perturbing these features, they create anomaly features and primarily train a discriminator over these normal and anomaly features. However, these methods lack robustness due to their reliance on highly vulnerable feature extractors and the absence of anomaly data in the input space, which prevents proper training of a robust feature extractor. The third category consists of DRAEM [89], NSA [68], Cutpaste [44], and GLASS [13], generate pseudo-anomaly data during training. Nevertheless, some of these methods lack access to masks or do not use a foreground-aware generation process. Despite their astonishing success in clean settings, we empirically show in Table 3 that even when adversarially trained, they exhibit unsatisfactory results. Furthermore, while anomaly localization has not been explored in an adversarial setup, some other works have pursued anomaly detection in an adversarial setting, including PrincipaLS [50], ZARND [58], and Rodeo [57]. These approaches have achieved relatively better results by incorporating pseudo-anomaly generation processes and adversarial training. However, their performance falls short in real-world high-resolution datasets (as presented in Table 1). For more details about previous works, see Appendix A.

3. Preliminaries

Anomaly Detection (AD) and Localization (AL): AD involves identifying instances that deviate from expected patterns, while AL focuses on localizing abnormal subregions within an image. In AD, a model assigns an anomaly score $S(x; f)$ to each sample x using model f ; if this score exceeds a predefined threshold, the sample is classified as anomalous. Conversely, lower scores indicate normal samples. In AL, a model generates an anomaly map $M(x; f)$ using model f , where each pixel of the map corresponds to an anomaly score for the respective pixel in the input image.

Adversarial Robustness of Anomaly Detectors: An adversarial attack, primarily studied within classification tasks, involves the malicious alteration of a data sample x with its label y into a new sample x^* that maximizes the loss function $\ell(x^*; y)$ [36, 81, 85]. This new sample x^* is known as an adversarial example of x , and the difference ($x^* - x$) is referred to as adversarial perturbation. To prevent significant semantic changes, the l_p norm of the adversarial noise is restricted by an upper limit ϵ . Specifically, an adversarial example x^* must satisfy the condition $x^* = \arg \max_{x': \|x-x'\|_p \leq \epsilon} \ell(x'; y)$. A widely used and effective attack method is the Projected Gradient Descent (PGD) [54] technique, which iteratively increases the loss function by moving in the direction of the gradient sign of

$\ell(x^*; y)$ with a specified step size α . When adapting adversarial attacks for AD, the objective shifts from maximizing the loss value to increasing $S(x, f)$ for normal samples and decreasing it for anomalies. The attack is formulated as $x_0^* = x$, $x_{t+1}^* = x_t^* + y \cdot \alpha \cdot \text{sign}(\nabla_x S(x_t^*; f_\theta))$, and $x^* = x_k^*$, where $y = +1$ for normal samples and $y = -1$ for anomaly samples. This approach is consistently applied to other attacks in the study [23, 85].

Adversarial Robustness of Anomaly Localization: Adversarial attacks aim to introduce perturbations that uniformly modify pixel scores in an anomaly map M , flipping scores from 0 to 1 or vice versa. In the context of AL, the attack objective transitions from merely maximizing a loss function to specifically increasing the values of $M(x, f)$ for normal samples while decreasing them for anomalies. The attack is formalized as follows: starting with $x_0^* = x$, the adversarial example at each step is updated as $x_{t+1}^* = x_t^* + Y \cdot \alpha \cdot \text{sign}(\nabla_x M(x_t^*; f_\theta))$, and the final adversarial example is $x^* = x_k^*$. Here, $Y_{i,j} = +1$ for normal pixels and $Y_{i,j} = -1$ for anomaly pixels, where i, j denote pixel coordinates. This strategy is extended to other advanced attack methods throughout the study [18]. Despite its significance, adversarial robustness in anomaly localization remains underexplored. Enhancing robustness is particularly critical for applications requiring spatial precision, such as medical diagnostics and industrial monitoring systems.

4. Theoretical Insights

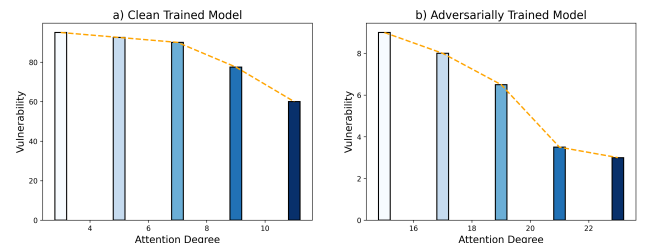


Figure 2. The figure demonstrates how increasing the average last-layer attention degree in the ViT-base architecture reduces vulnerability to adversarial attacks. Specifically, the BraTS dataset images were clustered into five groups based on their attention degree values (x-axis). The y-axis represents Vulnerability, measured as the absolute difference in the model’s localization performance (AUROC%) for each cluster before and after a PGD attack. (a) illustrates the decreasing trend in a clean-trained model. (b) shows a similar decreasing trend in the adversarially trained model, where the attention degree is relatively higher than in the clean model.

Here, we want to show why a self-attention layer, in which each token attends to a higher number of other tokens is more adversarially robust compared to the case that the attention is distributed over a smaller number of tokens.

Let’s consider the self-attention output embedding of the i th token in the l -th layer as $x_i^{(l)}$, and such embedding after the perturbation is applied to the input as $\hat{x}_i^{(l)}$. We are seeking to set $x_i^{(2)} - \hat{x}_i^{(2)} = r_i$, where r_i is the desired *adversarial direction* that most influences the layers next to the first layer of the transformer. According to the self-attention:

$$x_i^{(l+1)} = V^{(l)}.softmax(q_i^{(l)\top} K/\sqrt{d}),$$

where $q_i^{(l)} = W_q x_i^{(l)}$, $v_j^{(l)}$ the j -th column of $V^{(l)}$ be $v_j^{(l)} = W_v x_j^{(l)}$, $k_j^{(l)}$ the j -th column of K be $k_j^{(l)} = W_k x_j^{(l)}$, and d be the embedding dimension. For simplicity, we assume that the dimensions of embeddings of key, query, and values are all the same and are equal to the dimension of the original embeddings. Now, $W_v(X^{(1)}S - \hat{X}^{(1)}\hat{S}) = R$, where the columns of R and $X^{(1)}$ are represented by r_i and $x_i^{(1)}$, and the columns in S and \hat{S} correspond to the softmax values of each query token calculated for X and the perturbed inputs \hat{X} , respectively. Therefore,

$$\begin{aligned} W_v(X^{(1)}S - \hat{X}^{(1)}S) &= \\ W_v(X^{(1)}S - \hat{X}^{(1)}\hat{S} + \hat{X}^{(1)}\hat{S} - \hat{X}^{(1)}S) &= \\ R + W_v\hat{X}^{(1)}(\hat{S} - S) &= R + W_v\hat{X}^{(1)}\Delta S. \end{aligned}$$

where $\Delta S := \hat{S} - S$. Hence, we have:

$$X^{(1)} - \hat{X}^{(1)} = \underbrace{W_v^+(R + W_v\hat{X}^{(1)}\Delta S)}_U S^+.$$

Where W_v^+ and S^+ are the pseudo-inverses of the matrices W_v and S , respectively. Note that for the $\delta := X^{(1)} - \hat{X}^{(1)}$ perturbation in the input, in order to make the required perturbation in the output of the network, we get $\|\delta\| \leq \lambda_{max}\|U\|$, where λ_{max} is the maximum eigenvalue of S^+ . But we note that for a stochastic matrix S , the maximum eigenvalue is 1. Therefore, for the inverse matrix, S^+ , the maximum eigenvalue would be larger than 1. As a result, we would expect the $\|\delta\|$ to grow proportional to $\lambda_{max} \geq 1$. We note that the smaller $\|\delta\|$ would imply more vulnerability as it becomes easier to attack the network with a smaller perturbation length. On the other hand, for a purely localized S , where each token only attends to itself $\lambda_{max} = 1$, showing that the increase in $\|\delta\|$ would likely be small compared to the general case, leading to more vulnerability. Therefore, we conclude that a localized and overly sparse attention map would typically imply an easier attack on the network and hence higher vulnerability against adversarial attacks. Sparse attention values may also resemble what happens in convolutional networks that have small receptive fields.

5. Methodology

Overview. Current AD and AL methods perform poorly when subjected to adversarial attacks. Previous studies have

demonstrated the effectiveness of OE in enhancing robustness against such attacks [4, 11, 12, 57]. Additionally, ViTs have shown promising results in standard (clean) AD and AL tasks [16, 39, 45, 73], and our findings suggest their potential for adversarial settings with targeted modifications of attention degrees. Building on these insights and our theoretical foundations, we propose PatchGuard, a novel method designed to enhance adversarial robustness in AD and AL. The following subsections detail the key components of PatchGuard.

5.1. Foreground-Aware Pseudo-Anomaly Generation

To generate anomalous data from normal samples, it is essential to apply targeted distortions that ensure the image becomes anomalous [9, 14, 15, 28]. Additionally, the generated pseudo-anomalies must satisfy two key requirements: (1) inclusion of localization maps to enhance the AL task, and (2) close alignment with the normal sample distribution [57, 59]. Meeting these requirements simultaneously necessitates precise but minimal alterations within the foreground. Thus, the proposed method must reliably identify a region of the image that we can confidently attribute to the foreground.

To achieve this, we leverage insights from [63], which indicate that pretrained models benefit from style-agnostic processing to improve classification accuracy. To this end, we first introduce *soft transformations*, which are commonly used in self-supervised learning studies due to their ability to preserve semantic content [9, 14, 15, 28, 33]. Next, we apply Grad-CAM [69] to generate a saliency map using a standard pre-trained ResNet18 [32] model on a given input. Specifically, for a normal sample x , we randomly select k_{soft} soft transformations $t_1^s, \dots, t_{k_{soft}}^s$. We then compute saliency maps for $x, t_1^s(x), \dots, t_{k_{soft}}^s(x)$ and take their element-wise product to produce a style-invariant saliency map, $G(x)$. As shown in Figure 3 (part ①), $G(x)$ effectively assigns higher values to the foreground region.

To distort the obtained region, we first randomly sample an anchor point from it. We then sample k_{hard} hard transformations $t_1^h, \dots, t_{k_{hard}}^h$, which are typically associated with altering semantic integrity, as highlighted in prior research [1, 10, 20, 25, 35, 41, 44, 71, 72, 75, 86]. We then design a rectangular mask centered on this chosen point, with its width w and height h satisfying $w \sim U(0.05W, 0.3W)$ and $h \sim U(0.05H, 0.3H)$, where W and H are the image’s width and height. Next, we rotate the mask by an angle of $\theta \sim U(-45^\circ, 45^\circ)$. Finally, we sequentially apply the hard transformations only to the region within this mask, leaving the remaining unmasked areas of the image unchanged. Mathematically, the final anomaly is obtained by applying

$$x' = t_1^h(\dots(t_{k_{hard}}^h(x_{masked})\dots) + (x - x_{masked})). \quad (1)$$

An additional advantage of this pseudo-anomaly crafting ap-

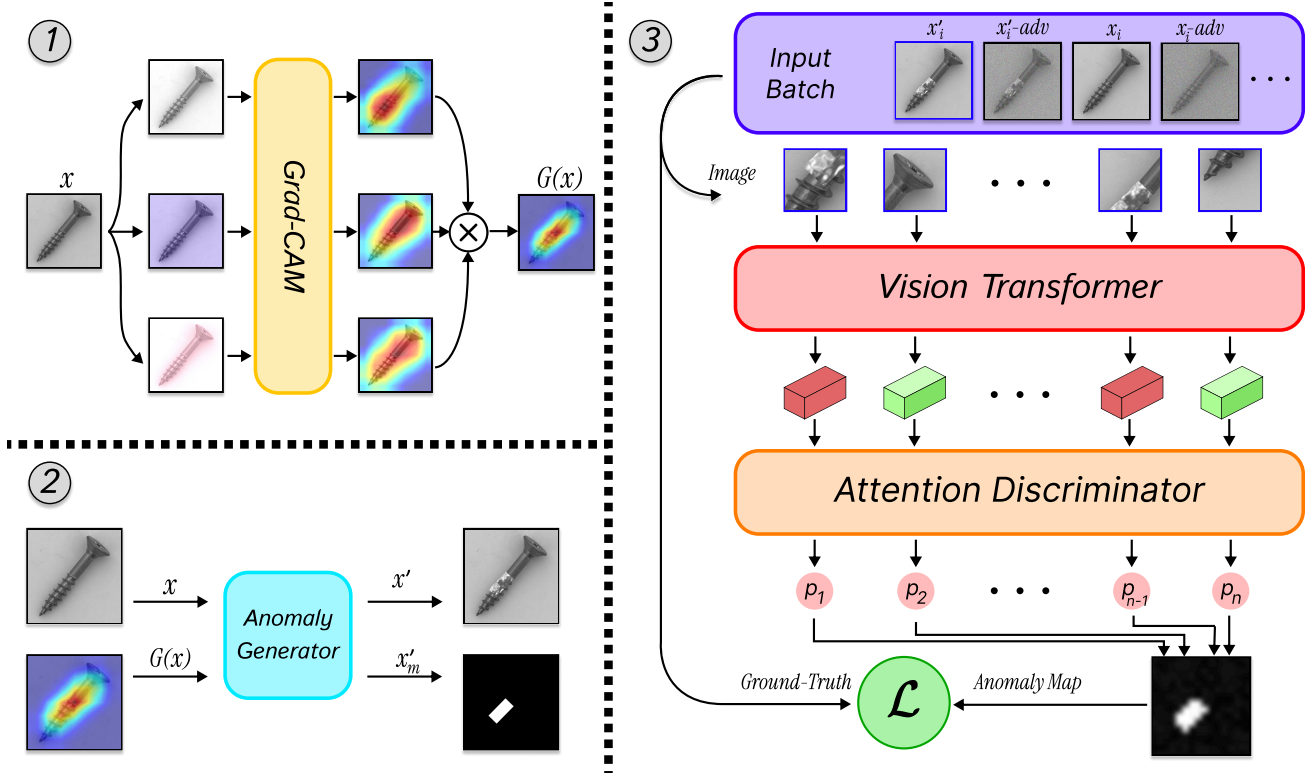


Figure 3. Overview of the PatchGuard framework. (1) We use Grad-CAM to identify regions likely to belong to the foreground in an image. By applying $k_{\text{soft}} = 3$ augmentations to the image x , we generate a combined saliency map $G(x)$. (2) The input x and its saliency map $G(x)$ are then passed to the anomaly generator to produce an anomaly sample x' along with its ground-truth mask x'_m . (3) For each normal sample x_i , the input batch includes the image, its corresponding anomaly version x'_i , and their adversarially attacked variants, along with their ground-truth masks. Each batch sample is processed through a Vision Transformer (ViT), where the Attention Discriminator assigns an anomaly score p_i to each patch embedding. The final anomaly map is constructed from these scores and trained with a novel loss \mathcal{L} to replicate the ground truth.

Table 1. Detection performance of various AD methods, including PatchGuard, across benchmark datasets. Results are shown as “Clean / Adversarial”, representing performance on “Clean” and “Adversarial” data (PGD-1000, $\epsilon = \frac{8}{255}$, measured by AUROC %), respectively.

Dataset	Method										
	DRAEM	PatchCore	SimpleNet	ReContrast	GeneralAD	GLAD	GLASS	PrincipaLS*	ZARND*	RODEO*	Ours
MVTec AD	98.0 / 5.1	99.1 / 3.9	99.6 / 2.3	99.5 / 0.0	99.2 / 13.7	99.3 / 11.8	99.9 / 6.7	63.8 / 10.6	71.6 / 11.0	61.5 / 4.9	88.1 / 71.1
VisA	88.7 / 3.8	95.1 / 1.7	96.2 / 0.2	97.5 / 6.7	95.9 / 14.5	99.5 / 8.6	98.8 / 7.2	58.9 / 9.3	67.7 / 9.3	63.1 / 3.8	88.5 / 74.3
BTAD	87.1 / 4.9	96.9 / 2.4	95.1 / 4.6	95.7 / 2.1	97.0 / 10.9	98.5 / 7.6	97.4 / 8.3	60.1 / 7.8	69.7 / 8.3	60.0 / 5.8	85.3 / 82.1
MPDD	94.3 / 2.8	91.3 / 6.8	96.6 / 7.0	94.5 / 4.5	98.0 / 12.8	97.5 / 9.7	99.6 / 9.1	71.9 / 15.7	65.7 / 12.2	68.8 / 7.4	85.4 / 68.6
WFDD	94.0 / 7.1	96.3 / 3.9	98.8 / 5.1	97.6 / 3.3	99.0 / 10.7	99.1 / 12.5	100 / 6.0	66.3 / 14.1	76.1 / 16.3	71.2 / 7.8	84.2 / 65.0
DTD-Synthetic	97.1 / 3.6	65.8 / 4.0	96.8 / 2.4	98.2 / 9.1	97.9 / 16.3	98.6 / 10.3	99.1 / 6.1	77.9 / 9.3	70.3 / 13.7	72.8 / 12.0	91.5 / 60.5
Head-CT	72.1 / 8.1	92.4 / 5.1	84.9 / 4.8	86.1 / 6.3	89.1 / 9.1	93.1 / 14.2	94.7 / 8.7	73.2 / 16.0	64.3 / 9.7	85.7 / 61.0	97.3 / 90.4
BraTS2021	62.3 / 1.4	91.6 / 6.3	82.5 / 6.1	82.4 / 3.1	88.3 / 13.0	92.3 / 12.0	95.7 / 7.2	75.3 / 8.7	66.7 / 14.0	89.1 / 64.7	94.3 / 81.0
Average	86.7 / 4.6	91.0 / 4.2	93.8 / 4.0	93.9 / 4.3	95.5 / 12.6	97.2 / 10.8	98.1 / 7.4	68.4 / 11.4	69.0 / 11.8	71.5 / 20.9	89.3 / 74.1

*These works incorporated adversarial training into their proposed AD methods.

Table 2. Localization performance of various AL methods, including PatchGuard, across benchmark datasets. Results are shown as “Clean / Adversarial”, representing performance on “Clean” and “Adversarial” data (PGD-1000, $\epsilon = \frac{8}{255}$, measured by AUROC %), respectively.

Dataset	Method										
	DRAEM	PatchCore	SimpleNet	ReContrast	GeneralAD	GLAD	GLASS	MuSc	ReConPatch	RealNet	Ours
MVTec AD	97.3 / 3.9	98.1 / 4.2	98.1 / 6.8	98.4 / 4.8	97.7 / 12.3	98.7 / 15.3	99.3 / 8.1	97.3 / 4.6	99.2 / 2.8	99.0 / 8.7	92.7 / 73.8
VisA	90.7 / 5.6	98.5 / 3.0	97.4 / 4.8	98.2 / 7.1	99.0 / 7.6	98.6 / 13.4	98.8 / 7.0	98.8 / 3.8	99.2 / 1.7	98.8 / 6.2	96.9 / 85.2
BTAD	89.0 / 7.1	92.6 / 6.3	95.2 / 3.7	96.8 / 6.4	96.7 / 9.3	98.2 / 14.5	97.0 / 5.7	97.3 / 5.3	97.5 / 3.0	97.9 / 9.2	93.2 / 73.0
MPDD	90.7 / 4.7	98.5 / 1.9	97.4 / 7.3	94.6 / 3.6	98.1 / 14.9	98.7 / 10.8	99.4 / 6.3	95.5 / 6.0	96.7 / 2.6	98.2 / 7.5	93.8 / 86.6
WFDD	95.8 / 3.9	98.1 / 2.1	98.0 / 3.4	97.3 / 5.1	98.7 / 13.5	97.6 / 11.3	98.9 / 7.6	97.0 / 4.1	98.3 / 4.9	98.4 / 6.8	94.6 / 71.6
DTD-Synthetic	96.1 / 4.8	95.6 / 6.7	97.0 / 2.9	96.8 / 7.6	97.9 / 10.8	97.3 / 13.8	98.1 / 7.0	97.8 / 5.7	96.3 / 3.9	98.0 / 8.3	95.9 / 74.8
Head-CT	86.4 / 8.9	87.3 / 6.1	89.7 / 0.8	90.1 / 8.6	91.7 / 18.3	93.4 / 16.7	92.2 / 9.1	85.2 / 8.5	89.7 / 6.6	94.8 / 7.3	93.6 / 89.3
BraTS2021	82.2 / 6.1	96.9 / 4.5	94.7 / 6.7	95.3 / 11.1	96.8 / 14.7	95.1 / 13.5	94.0 / 6.3	67.5 / 6.3	97.5 / 5.9	96.9 / 10.2	97.7 / 94.5
Average	91.0 / 5.6	95.7 / 4.3	95.9 / 4.5	95.9 / 6.7	97.0 / 12.6	97.2 / 13.6	97.2 / 7.1	92.0 / 5.5	96.8 / 3.9	97.7 / 8.0	94.8 / 81.1

proach is that the location of the distorted region is precisely known, allowing us to generate an accurate localization map x'_m for AL training, where each pixel’s value equals 1 if it’s anomalous, and 0 otherwise. By creating an anomalous counterpart x' and its corresponding localization map x'_m for each normal sample x in the training set, we provide the model with both the anomaly and its location, as shown in Figure 3 (part ②). This pairing equips the model with the information needed to improve its localization accuracy, as we will discuss in Section 5.2. For details on the soft and hard transforms, and ablations on the hypers used in this approach, refer to Table 6 and Appendix B.

5.2. Anomaly Detection and Localization with Vision Transformer

To enhance adversarial robustness through the effective use of pseudo-anomaly samples and their corresponding localization maps, we employ a Vision Transformer (ViT) model. This model generates output embeddings that are processed by an attention-based discriminator network, which uses a multi-head attention (MLH) mechanism followed by a shared-weight multi-layer perceptron (MLP). The discriminator independently assigns an anomaly score to each patch in the input, providing a patch-level anomaly prediction as shown in Figure 3 (part ③).

The model is trained using a combination of patch-level cross-entropy (CE) and an additional regularization term R , designed to encourage a higher degree of attention in a specified ViT layer. As illustrated in Figure 2 and the theory in Section 4, this regularizer is expected to further enhance adversarial robustness. The cross-entropy loss component aligns the predicted anomaly scores with ground truth labels from the localization map, x_m , where a patch label equals 1 if more than 5% of the pixels in the corresponding patch in

x_m are anomalous, and 0 otherwise:

$$M = \text{MLP}(\text{MLH}(x)) \quad (2)$$

$$\mathcal{L}_{\text{CE}}(x, x_m) = \sum_{i,j \in x_{\text{patches}}} \text{CE}(M_{(i,j)}, x_{m,(i,j)}) \quad (3)$$

Here, M denotes the predicted AL map, consisting of anomaly scores for each patch, x is any input sample (normal or anomaly), and i, j are the indices for individual patches. The cross-entropy loss term \mathcal{L}_{CE} ensures alignment between the patch $M_{(i,j)}$ and the ground truth anomaly map $x_{m,(i,j)}$, promoting precise anomaly localization. The final AL map is obtained by upsampling M to the original image size, and we use the average of the top- k patch-level anomaly scores as the image-level anomaly score.

To further improve the robustness of the model, we introduce a regularization term R , which encourages an increased attention degree in a specified layer ℓ of the ViT, chosen here as the final layer. This regularization term is formulated as:

$$R(x) = \frac{1}{\sum_i \sum_j \sum_k A_{ijk} \cdot \mathbb{1}(A_{ijk} \leq \delta)} \quad (4)$$

Here, A_{ijk} represents the attention coefficient corresponding to the i -th head, the j -th output patch, and the k -th input patch. Regularization will increase the values of attention coefficients that are below the threshold δ . For a specific output patch, since a softmax function is applied to its corresponding attention coefficients, increasing the lower values naturally decreases the higher ones. With $\delta = \frac{1}{(\text{number of input patches})}$, the coefficient distribution gradually shifts toward a uniform distribution at this threshold, representing the maximum attention degree a patch can achieve. The total loss function \mathcal{L} used for training the model is the

sum of the cross-entropy and the regularization term:

$$\mathcal{L}(x, x_m) = \mathcal{L}_{\text{CE}}(x, x_m) + \alpha R(x) \quad (5)$$

where α is a scaling factor that controls the strength of the regularization. This combined objective encourages the model to not only accurately predict anomaly locations but also maintain an increased level of attention, enhancing both detection performance and adversarial robustness. It is then used in adversarial training, as explained in Section 5.3. Comprehensive ablation studies of hyperparameters including δ and α are provided in Appendix C.2 and Section 7.

5.3. Adversarial Training and Testing

Given an input sample x , an adversarial example x_{adv} is generated by introducing a perturbation δ^* , optimized to maximize the final loss:

$$\delta^* = \underset{\|\delta\|_{\infty} \leq \epsilon}{\operatorname{argmax}} \mathcal{L}(x + \delta, x_m), \quad x_{adv} = x + \delta^* \quad (6)$$

These adversarial examples are then used in the training process alongside the original examples. The adversarial training objective is framed as a min-max problem, optimizing the model parameters θ to minimize the expected loss over both clean and adversarial examples:

$$\min_{\theta} \mathbb{E}_{(x,y) \in \mathcal{B}} \left[\max_{\|\delta\|_{\infty} \leq \epsilon} \mathcal{L}(x + \delta, x_m; \theta) \right]. \quad (7)$$

6. Experiments

To demonstrate the effectiveness of PatchGuard, we conduct extensive experiments assessing its performance alongside several established anomaly detection methods on multiple benchmarks for anomaly detection and localization. Our evaluation includes both adversarially trained models and those trained under standard conditions. To ensure a fair comparison, we assess all methods under both ‘‘Clean’’ and ‘‘Adversarial’’ test conditions, as shown in Table 1 and 2. In the Clean setting, test samples are unaltered, whereas the Adversarial setting includes samples perturbed by the PGD attack [54]. Additional results on PatchGuard’s performance against alternative attacks are provided in Section 7.2. Datasets are detailed in Appendix D.

Evaluation Details. In the adversarial setting, we evaluate each method using the ℓ_{∞} PGD-1000 attack with $\epsilon = \frac{8}{255}$. Detection and localization results are shown in Tables 1 and 2, respectively. ℓ_2 norm evaluations are in Appendix J.

Adapting State-of-the-Art AD and AL Methods to Adversarial Settings. Prior to developing our novel PatchGuard framework, we first investigated whether existing state-of-the-art methods in AD and AL could be enhanced through adversarial training—a technique where models are

Table 3. Performance of prior methods adapted for adversarial settings, shown as ‘‘Clean / Adversarial’’ (PGD-1000, $\epsilon = \frac{8}{255}$).

Method	Task	Dataset			
		MVTec AD	VisA	BTAD	BraTS2021
PatchCore	AD	92.3 / 14.3	88.4 / 10.8	87.1 / 12.7	88.6 / 16.1
	AL	89.1 / 10.3	87.6 / 8.8	85.0 / 11.5	86.7 / 13.6
ReContrast	AD	93.8 / 5.1	93.7 / 16.7	89.9 / 13.4	78.2 / 13.1
	AL	94.5 / 17.2	92.5 / 18.2	88.6 / 17.9	90.8 / 14.2
SimpleNet	AD	91.1 / 18.1	89.2 / 14.9	88.6 / 12.7	75.3 / 14.2
	AL	94.1 / 19.5	89.4 / 15.8	88.2 / 11.7	90.1 / 17.0
GeneralAD	AD	84.6 / 24.7	81.2 / 22.1	82.9 / 20.6	80.7 / 19.9
	AL	83.7 / 21.8	83.1 / 17.3	84.7 / 18.3	79.6 / 21.0
DRAEM	AD	83.0 / 19.2	81.7 / 16.8	79.1 / 17.0	57.4 / 12.2
	AL	86.1 / 17.5	78.6 / 15.0	80.9 / 18.6	73.6 / 14.9
GLASS	AD	84.2 / 26.7	83.5 / 19.9	84.7 / 25.4	83.7 / 20.1
	AL	85.9 / 21.2	87.1 / 21.7	83.0 / 19.0	85.8 / 23.6
Ours	AD	88.1 / 71.1	88.5 / 74.3	85.3 / 82.1	94.3 / 81.0
	AL	92.7 / 73.8	96.9 / 85.2	93.2 / 73.0	97.7 / 94.5

trained on adversarial examples to improve their robustness. In Appendix E, we provide a detailed methodology for generating adversarial examples for each method and describe our optimized approach for improving their resilience. The empirical results, presented in Table 3, reveal that even after incorporating adversarial training, current SOTA AD and AL methods remain vulnerable to adversarial attacks and exhibit suboptimal performance. These limitations motivated the development of PatchGuard, our proposed solution.

Analyzing Results. As shown in Tables 1 and 2, prior SOTA methods such as Recontrast demonstrate substantial drops in performance under adversarial settings, despite excelling in clean conditions. Furthermore, as indicated in Table 3, even when adversarially trained, these methods struggle to achieve robust performance. By contrast, approaches specifically designed to address adversarial robustness, such as RODEO, still fall short when compared to PatchGuard. On average, PatchGuard improves robust detection across diverse datasets by up to 53.2% percent, with a notable robust improvement of 68.5% percent on the challenging MVTEC dataset. Notably, we achieve a 71.8% improvement in AL on the challenging VisA dataset, with details in Appendix F. As prior research indicates, a slight decrease in clean performance is generally viewed as an acceptable tradeoff for the critical gains in robustness.

Implementation Details. We leverage a from-scratch ViT model in our pipeline to showcase our setup’s independence from pre-train datasets. However, we conduct an ablation study on this manner in Appendix C.4. Further, we leverage PGD-10 with $\epsilon = \frac{8}{255}$ for adversarial training,

Table 4. Evaluation of PatchGuard’s performance against advanced classification and segmentation attacks, showcasing its robustness in diverse attack scenarios.

Dataset	Task	Detection Attacks				Localization Attacks	
		PGD-1000	CAA	AutoAttack	A ³	SegPGD	SEA
MVTec AD	AD	71.1	74.8	70.8	69.8	71.9	69.2
	AL	73.8	76.7	72.9	70.0	74.6	71.3
VisA	AD	74.3	78.5	74.6	73.1	75.0	73.6
	AL	85.2	87.4	85.5	84.7	85.0	83.7
BTAD	AD	82.1	83.4	82.0	80.7	81.9	80.8
	AL	73.0	74.7	72.3	71.5	72.9	71.1
BraTS2021	AD	81.0	84.7	81.9	80.3	82.0	81.1
	AL	94.5	95.0	94.2	93.8	94.8	93.4

Table 5. Ablation study on the scaling factor α , illustrating the effectiveness of our regularization.

Scaling Factor (α)	Task	Dataset			
		MVTec-AD	VisA	BTAD	BraTS2021
0	AD	89.3 / 60.7	90.1 / 62.9	88.6 / 74.3	95.2 / 72.0
	AL	93.5 / 65.3	95.8 / 72.1	94.0 / 59.7	98.2 / 83.4
1 (Ours)	AD	88.1 / 71.1	88.5 / 74.3	85.3 / 82.1	94.3 / 81.0
	AL	92.7 / 73.8	96.9 / 85.2	93.2 / 73.0	97.7 / 94.5
2	AD	86.2 / 70.1	87.6 / 75.1	84.7 / 83.4	92.8 / 81.2
	AL	91.0 / 68.9	94.8 / 84.1	91.9 / 73.9	95.8 / 94.6
5	AD	80.1 / 64.1	78.6 / 65.4	73.8 / 69.6	82.5 / 73.2
	AL	84.7 / 65.6	81.1 / 78.9	84.0 / 65.3	86.3 / 79.9

but the test results are generated with the PGD-1000 attack. For more details on the implementation parameters, refer to Appendix G.

7. Ablation Studies

In this section, we provided further analysis of our choices of parameters and other components of our method.

7.1. Regularization

To experimentally demonstrate the effectiveness of our regularization term on the model’s robustness and the impact of the scaling factor α (set to 1 by default in our method), we conduct an ablation study on α , as shown in Table 5. When $\alpha = 0$, the model’s robustness against adversarial attacks decreases due to the lack of regularization. On the other hand, higher values of α , such as $\alpha = 5$, cause the regularization term to dominate, leading to an unstable loss function and inappropriate results.

7.2. Advanced Attacks

In our primary experiments in Section 6, we utilized variations of the PGD attack [54] for both model training and

Table 6. An ablation study on our method’s performance using various anomaly generation techniques that incorporate masks.

Pseudo-Anomaly Generator	Task	Dataset			
		MVTec AD	VisA	BTAD	BraTS2021
CutPaste	AD	79.1 / 60.3	74.4 / 61.5	74.8 / 69.2	80.3 / 72.7
	AL	83.9 / 60.8	85.4 / 73.0	82.6 / 61.2	91.2 / 82.1
FPI	AD	78.9 / 62.1	75.1 / 64.3	72.9 / 71.0	84.1 / 74.1
	AL	84.3 / 63.8	82.9 / 71.8	86.3 / 60.5	93.3 / 84.8
NSA	AD	81.7 / 66.5	83.1 / 65.4	77.1 / 73.4	86.3 / 73.8
	AL	85.1 / 65.0	83.3 / 76.7	85.4 / 64.9	89.4 / 86.8
GLASS	AD	83.2 / 62.0	84.0 / 68.7	79.3 / 73.9	83.1 / 66.1
	AL	86.7 / 67.0	86.2 / 78.5	86.8 / 68.2	92.2 / 87.3
Ours	AD	88.1 / 71.1	88.5 / 74.3	85.3 / 82.1	94.3 / 81.0
	AL	92.7 / 73.8	96.9 / 85.2	93.2 / 73.0	97.7 / 94.5

testing. To further illustrate the adaptability and robustness of our proposed method under diverse adversarial conditions, we also evaluate its performance against a variety of other attack types including Detection attacks and Localization attacks. The Detection attacks consist of black-box attacks [30], FGSM [26], CAA [55], AutoAttack [17], and A³ (Adversarial Attack Automation) [48]. The localization attacks are adapted from the well-known segmentation attacks in literature, namely SegPGD [29] and SEA [18]. All results are available in Table 4, and the exact details on our adaptation approach for these attacks are available in Appendix H. It is important to note that the training process remains consistent, employing only the standard PGD-10 for simplicity and practicality.

7.3. Pseudo-Anomaly Generation Strategy

Since our method targets both AD and AL using pseudo-anomalies, it is crucial to evaluate our pseudo-anomaly generation against compatible methods that produce localization maps. Thus, methods like MIXUP [35], FakeIt [56], and Dream-OOD [22] are excluded. We compare instead with CutPaste [44], NSA [68], GLASS [13], and FPI [76], keeping other pipeline components fixed. As shown in Table 6, our method outperforms these approaches, highlighting its effectiveness for robust anomaly localization.

8. Conclusion

We introduce PatchGuard, an adversarially robust method for AD and AL. It employs Foreground-Aware Pseudo-Anomaly Generation using segmentation masks. Additionally, we propose a regularization term, motivated by observations and theory, that strengthens robustness against adversarial attacks by increasing the attention degree. PatchGuard outperforms previous methods on AD and AL benchmarks under adversarial settings.

Acknowledgments

We are very grateful to Mohammad Javad Maheron-naghsh for his collaboration in the initial stages of this project and to the anonymous reviewers for their helpful discussions and valuable feedback.

References

- [1] M. Eren Akbiyik. Data augmentation in training cnns: Injecting noise to images. *ArXiv*, abs/2307.06855, 2019. 4
- [2] Naveed Akhtar and Ajmal Mian. Threat of adversarial attacks on deep learning in computer vision: A survey. *Ieee Access*, 6:14410–14430, 2018. 1
- [3] Toshimichi Aota, Lloyd Teh Tzer Tong, and Takayuki Okatani. Zero-shot versus many-shot: Unsupervised texture anomaly detection. In *Proceedings of the IEEE/CVF Winter Conference on Applications of Computer Vision (WACV)*, pages 5564–5572, 2023. 3
- [4] Mohammad Azizmalayeri, Arshia Soltani Moakhar, Arman Zarei, Reihaneh Zohrabi, Mohammad Manzuri, and Mohammad Hossein Rohban. Your out-of-distribution detection method is not robust! *Advances in Neural Information Processing Systems*, 35:4887–4901, 2022. 1, 2, 4
- [5] Ujjwal Baid, Satyam Ghodasara, Suyash Mohan, Michel Bilello, Evan Calabrese, Errol Colak, Keyvan Farahani, Jayashree Kalpathy-Cramer, Felipe C Kitamura, Sarthak Pati, et al. The rsna-asnr-miccai brats 2021 benchmark on brain tumor segmentation and radiogenomic classification. *arXiv preprint arXiv:2107.02314*, 2021. 2
- [6] Abhijit Bendale and Terrance Boulton. Towards open world recognition. In *Proceedings of the IEEE Conference on Computer Vision and Pattern Recognition (CVPR)*, pages 1893–1902, 2015. 2
- [7] Paul Bergmann, Michael Fauser, David Sattlegger, and Carsten Steger. Mvtec ad—a comprehensive real-world dataset for unsupervised anomaly detection. In *Proceedings of the IEEE/CVF conference on computer vision and pattern recognition*, pages 9592–9600, 2019. 1, 2
- [8] Louis Béthune, Paul Novello, Thibaut Boissin, Guillaume Coiffier, Mathieu Serrurier, Quentin Vincenot, and Andres Troya-Galvis. Robust one-class classification with signed distance function using 1-lipschitz neural networks. *arXiv preprint arXiv:2303.01978*, 2023. 1
- [9] Mathilde Caron, Ishan Misra, Julien Mairal, Priya Goyal, Piotr Bojanowski, and Armand Joulin. Unsupervised learning of visual features by contrasting cluster assignments. *Advances in neural information processing systems*, 33:9912–9924, 2020. 4, 3
- [10] Chengwei Chen, Yuan Xie, Shaohui Lin, Ruizhi Qiao, Jian Zhou, Xin Tan, Yi Zhang, and Lizhuang Ma. Novelty detection via contrastive learning with negative data augmentation. In *Proceedings of the Thirtieth International Joint Conference on Artificial Intelligence, IJCAI 2021, Virtual Event / Montreal, Canada, 19-27 August 2021*, pages 606–614. ijcai.org, 2021. 4
- [11] Jiefeng Chen, Yixuan Li, Xi Wu, Yingyu Liang, and Somesh Jha. Robust out-of-distribution detection for neural networks. *arXiv preprint arXiv:2003.09711*, 2020. 1, 2, 4
- [12] Jiefeng Chen, Yixuan Li, Xi Wu, Yingyu Liang, and Somesh Jha. Atom: Robustifying out-of-distribution detection using outlier mining. In *Machine Learning and Knowledge Discovery in Databases. Research Track: European Conference, ECML PKDD 2021, Bilbao, Spain, September 13–17, 2021, Proceedings, Part III 21*, pages 430–445. Springer, 2021. 2, 4
- [13] Qiyu Chen, Huiyuan Luo, Chengkan Lv, and Zhengtao Zhang. A unified anomaly synthesis strategy with gradient ascent for industrial anomaly detection and localization. *arXiv preprint arXiv:2407.09359*, 2024. 1, 3, 8, 4
- [14] Ting Chen, Simon Kornblith, Mohammad Norouzi, and Geoffrey Hinton. A simple framework for contrastive learning of visual representations. In *International conference on machine learning*, pages 1597–1607. PMLR, 2020. 4
- [15] Xinlei Chen and Kaiming He. Exploring simple siamese representation learning. In *Proceedings of the IEEE/CVF conference on computer vision and pattern recognition*, pages 15750–15758, 2021. 4
- [16] Matan Jacob Cohen and Shai Avidan. Transformalys—two (feature spaces) are better than one. *arXiv preprint arXiv:2112.04185*, 2021. 2, 4, 1
- [17] Francesco Croce and Matthias Hein. Reliable evaluation of adversarial robustness with an ensemble of diverse parameter-free attacks. In *International conference on machine learning*, pages 2206–2216. PMLR, 2020. 8
- [18] Francesco Croce, Naman D Singh, and Matthias Hein. Towards reliable evaluation and fast training of robust semantic segmentation models. In *ECCV*, 2024. 2, 3, 8
- [19] Jia Deng, Wei Dong, Richard Socher, Li-Jia Li, Kai Li, and Li Fei-Fei. Imagenet: A large-scale hierarchical image database. In *2009 IEEE Conference on Computer Vision and Pattern Recognition*, pages 248–255. IEEE, 2009. 4
- [20] Terrance DeVries and Graham W Taylor. Improved regularization of convolutional neural networks with cutout. *arXiv preprint arXiv:1708.04552*, 2017. 4
- [21] Alexey Dosovitskiy, Lucas Beyer, Alexander Kolesnikov, Dirk Weissenborn, Xiaohua Zhai, Thomas Unterthiner, Mostafa Dehghani, Matthias Minderer, Georg Heigold, Sylvain Gelly, et al. An image is worth 16x16 words: Transformers for image recognition at scale. *arXiv preprint arXiv:2010.11929*, 2020. 2
- [22] Xuefeng Du, Yiyu Sun, Xiaojin Zhu, and Yixuan Li. Dream the impossible: Outlier imagination with diffusion models. *arXiv preprint arXiv:2309.13415*, 2023. 8
- [23] Reuben Feinman, Ryan R Curtin, Saurabh Shintre, and Andrew B Gardner. Detecting adversarial samples from artifacts. *arXiv preprint arXiv:1703.00410*, 2017. 3
- [24] Tharindu Fernando, Harshala Gammulle, Simon Denman, Sridha Sridharan, and Clinton Fookes. Deep learning for medical anomaly detection—a survey. *ACM Computing Surveys (CSUR)*, 54(7):1–37, 2021. 1
- [25] Golnaz Ghiasi, Yin Cui, Aravind Srinivas, Rui Qian, Tsung-Yi Lin, Ekin D Cubuk, Quoc V Le, and Barret Zoph. Simple copy-paste is a strong data augmentation method for instance segmentation. *arXiv preprint arXiv:2012.07177*, 2020. 4

- [26] Ian J Goodfellow, Jonathon Shlens, and Christian Szegedy. Explaining and harnessing adversarial examples. *arXiv preprint arXiv:1412.6572*, 2014. 1, 8
- [27] Adam Goodge, Bryan Hooi, See Kiong Ng, and Wee Siong Ng. Robustness of autoencoders for anomaly detection under adversarial impact. In *Proceedings of the Twenty-Ninth International Conference on International Joint Conferences on Artificial Intelligence*, pages 1244–1250, 2021. 1
- [28] Jean-Bastien Grill, Florian Strub, Florent Altché, Corentin Tallec, Pierre Richemond, Elena Buchatskaya, Carl Doersch, Bernardo Avila Pires, Zhaohan Guo, Mohammad Gheshlaghi Azar, et al. Bootstrap your own latent—a new approach to self-supervised learning. *Advances in neural information processing systems*, 33:21271–21284, 2020. 4
- [29] Jindong Gu, Hengshuang Zhao, Volker Tresp, and Philip HS Torr. Segpgd: An effective and efficient adversarial attack for evaluating and boosting segmentation robustness. In *European Conference on Computer Vision*, pages 308–325. Springer, 2022. 8
- [30] Chuan Guo, Jacob Gardner, Yurong You, Andrew Gordon Wilson, and Kilian Weinberger. Simple black-box adversarial attacks. In *International Conference on Machine Learning*, pages 2484–2493. PMLR, 2019. 8
- [31] Jia Guo, Lize Jia, Weihang Zhang, Huiqi Li, et al. Recontrast: Domain-specific anomaly detection via contrastive reconstruction. *Advances in Neural Information Processing Systems*, 36, 2024. 2, 1, 3
- [32] Kaiming He, Xiangyu Zhang, Shaoqing Ren, and Jian Sun. Deep residual learning for image recognition. In *2016 IEEE Conference on Computer Vision and Pattern Recognition (CVPR)*, pages 770–778, 2016. 4, 2, 3
- [33] Kaiming He, Haoqi Fan, Yuxin Wu, Saining Xie, and Ross Girshick. Momentum contrast for unsupervised visual representation learning. In *Proceedings of the IEEE/CVF conference on computer vision and pattern recognition*, pages 9729–9738, 2020. 4
- [34] Dan Hendrycks, Mantas Mazeika, and Thomas Dietterich. Deep anomaly detection with outlier exposure. *arXiv preprint arXiv:1812.04606*, 2018. 2
- [35] Yann N. Dauphin Hongyi Zhang, Moustapha Cisse. mixup: Beyond empirical risk minimization. *International Conference on Learning Representations*, 2018. 4, 8
- [36] Mohammad Hossein Rohban Hossein Mirzaei, ... Scanning trojaned models using out-of-distribution samples. In *Advances in Neural Information Processing Systems*, 2024. 3
- [37] Jiande Huang, Xingxing Li, Xin Li, Jiaqi Wu, Keke Zhang, Yongqiang Yuan, and Wei Zhang. Real-time outlier detection of satellite orbit and clock products using reverse error estimation. *GPS Solutions*, 29(1):2, 2025. 2
- [38] Nicholas Jeffrey, Qing Tan, and José R Villar. A review of anomaly detection strategies to detect threats to cyber-physical systems. *Electronics*, 12(15):3283, 2023. 1
- [39] Jongheon Jeong, Yang Zou, Taewan Kim, Dongqing Zhang, Avinash Ravichandran, and Onkar Dabeer. Winclip: Zero/few-shot anomaly classification and segmentation. In *Proceedings of the IEEE/CVF Conference on Computer Vision and Pattern Recognition*, pages 19606–19616, 2023. 2, 4
- [40] Stepan Jezek, Martin Jonak, Radim Burget, Pavel Dvorak, and Milos Skotak. Deep learning-based defect detection of metal parts: evaluating current methods in complex conditions. In *2021 13th International Congress on Ultra Modern Telecommunications and Control Systems and Workshops (ICUMT)*, pages 66–71, 2021. 3
- [41] Yannis Kalantidis, Mert Bulent Sariyildiz, Noe Pion, Philippe Weinzaepfel, and Diane Larlus. Hard negative mixing for contrastive learning. *Advances in Neural Information Processing Systems*, 33:21798–21809, 2020. 4
- [42] F.C. Kitamura. Head ct - hemorrhage, 2018. 3
- [43] Jungbeom Lee, Eunji Kim, Jisoo Mok, and Sungroh Yoon. Anti-adversarially manipulated attributions for weakly supervised semantic segmentation and object localization. *IEEE transactions on pattern analysis and machine intelligence*, 46(3):1618–1634, 2022. 2
- [44] Chun-Liang Li, Kihyuk Sohn, Jinsung Yoon, and Tomas Pfister. Cutpaste: Self-supervised learning for anomaly detection and localization. In *Proceedings of the IEEE/CVF Conference on Computer Vision and Pattern Recognition*, pages 9664–9674, 2021. 3, 4, 8
- [45] Xurui Li, Ziming Huang, Feng Xue, and Yu Zhou. Musc: Zero-shot industrial anomaly classification and segmentation with mutual scoring of the unlabeled images. *arXiv preprint arXiv:2401.16753*, 2024. 2, 4
- [46] T Lin. Focal loss for dense object detection. *arXiv preprint arXiv:1708.02002*, 2017. 4
- [47] Jiaqi Liu, Guoyang Xie, Jinbao Wang, Shangnian Li, Chengjie Wang, Feng Zheng, and Yaochu Jin. Deep industrial image anomaly detection: A survey. *Machine Intelligence Research*, 21(1):104–135, 2024. 1
- [48] Ye Liu, Yaya Cheng, Lianli Gao, Xianglong Liu, Qilong Zhang, and Jingkuan Song. Practical evaluation of adversarial robustness via adaptive auto attack, 2022. 2, 8
- [49] Zhikang Liu, Yiming Zhou, Yuansheng Xu, and Zilei Wang. SimpNet: A simple network for image anomaly detection and localization. In *Proceedings of the IEEE/CVF Conference on Computer Vision and Pattern Recognition*, pages 20402–20411, 2023. 3
- [50] Shao-Yuan Lo, Poojan Oza, and Vishal M Patel. Adversarially robust one-class novelty detection. *IEEE Transactions on Pattern Analysis and Machine Intelligence*, 2022. 1, 3
- [51] Ilya Loshchilov and Frank Hutter. Decoupled weight decay regularization. In *International Conference on Learning Representations*, 2019. 4
- [52] Pauline Luc, Camille Couprie, Soumith Chintala, and Jakob Verbeek. Semantic segmentation using adversarial networks. *arXiv preprint arXiv:1611.08408*, 2016. 2
- [53] Yuan Luo, Ya Xiao, Long Cheng, Guojun Peng, and Danfeng Yao. Deep learning-based anomaly detection in cyber-physical systems: Progress and opportunities. *ACM Computing Surveys (CSUR)*, 54(5):1–36, 2021. 1
- [54] Aleksander Madry, Aleksandar Makelov, Ludwig Schmidt, Dimitris Tsipras, and Adrian Vladu. Towards deep learning models resistant to adversarial attacks. *arXiv preprint arXiv:1706.06083*, 2017. 1, 2, 3, 7, 8

- [55] Xiaofeng Mao, Yuefeng Chen, Shuhui Wang, Hang Su, Yuan He, and Hui Xue. Composite adversarial attacks. *ArXiv*, abs/2012.05434, 2020. 8
- [56] Hossein Mirzaei, Mohammadreza Salehi, Sajjad Shahabi, Efstratios Gavves, Cees GM Snoek, Mohammad Sabokrou, and Mohammad Hossein Rohban. Fake it till you make it: Near-distribution novelty detection by score-based generative models. *arXiv preprint arXiv:2205.14297*, 2022. 8
- [57] Hossein Mirzaei, Mohammad Jafari, Hamid Reza Dehbashi, Ali Ansari, Sepehr Ghobadi, Masoud Hadi, Arshia Soltani Moakhar, Mohammad Azizmalayeri, Mahdiah Soleymani Baghshah, and Mohammad Hossein Rohban. Rodeo: Robust outlier detection via exposing adaptive out-of-distribution samples. In *Forty-first International Conference on Machine Learning*, 2024. 1, 2, 3, 4
- [58] Hossein Mirzaei, Mohammad Jafari, Hamid Reza Dehbashi, Zeinab Sadat Taghavi, Mohammad Sabokrou, and Mohammad Hossein Rohban. Killing it with zero-shot: Adversarially robust novelty detection. In *ICASSP 2024-2024 IEEE International Conference on Acoustics, Speech and Signal Processing (ICASSP)*, pages 7415–7419. IEEE, 2024. 3
- [59] Hossein Mirzaei, Mojtaba Nafez, Mohammad Jafari, Mohammad Bagher Soltani, Mohammad Azizmalayeri, Jafar Habibi, Mohammad Sabokrou, and Mohammad Hossein Rohban. Universal novelty detection through adaptive contrastive learning. In *Proceedings of the IEEE/CVF Conference on Computer Vision and Pattern Recognition*, pages 22914–22923, 2024. 4
- [60] Hossein Mirzaei, Mojtaba Nafez, Jafar Habibi, Mohammad Sabokrou, and Mohammad Hossein Rohban. Mitigating spurious negative pairs for robust industrial anomaly detection, 2025. 2
- [61] Pankaj Mishra, Riccardo Verk, Daniele Fornasier, Claudio Piciarelli, and Gian Luca Foresti. VT-ADL: A vision transformer network for image anomaly detection and localization. In *30th IEEE/IES International Symposium on Industrial Electronics (ISIE)*, 2021. 3
- [62] Arian Mousakhan, Thomas Brox, and Jawad Tayyub. Anomaly detection with conditioned denoising diffusion models. *arXiv preprint arXiv:2305.15956*, 2023. 1
- [63] Fahimeh Hosseini Noohdani, Parsa Hosseini, Aryan Yazdan Parast, Hamidreza Yaghoubi Araghi, and Mahdiah Soleymani Baghshah. Decompose-and-compose: A compositional approach to mitigating spurious correlation. In *Proceedings of the IEEE/CVF Conference on Computer Vision and Pattern Recognition*, pages 27662–27671, 2024. 2, 4
- [64] Pramuditha Perera, Poojan Oza, and Vishal M Patel. One-class classification: A survey. *arXiv preprint arXiv:2101.03064*, 2021. 2
- [65] Olaf Ronneberger, Philipp Fischer, and Thomas Brox. U-net: Convolutional networks for biomedical image segmentation. In *Medical image computing and computer-assisted intervention—MICCAI 2015: 18th international conference, Munich, Germany, October 5-9, 2015, proceedings, part III 18*, pages 234–241. Springer, 2015. 2
- [66] Karsten Roth, Latha Pemula, Joaquin Zepeda, Bernhard Schölkopf, Thomas Brox, and Peter Gehler. Towards total recall in industrial anomaly detection, 2021. 2, 3
- [67] Mohammadreza Salehi, Hossein Mirzaei, Dan Hendrycks, Yixuan Li, Mohammad Hossein Rohban, and Mohammad Sabokrou. A unified survey on anomaly, novelty, open-set, and out-of-distribution detection: Solutions and future challenges. *arXiv preprint arXiv:2110.14051*, 2021. 2
- [68] Hannah M Schlüter, Jeremy Tan, Benjamin Hou, and Bernhard Kainz. Natural synthetic anomalies for self-supervised anomaly detection and localization. In *European Conference on Computer Vision*, pages 474–489. Springer, 2022. 3, 8
- [69] Ramprasaath R Selvaraju, Michael Cogswell, Abhishek Das, Ramakrishna Vedantam, Devi Parikh, and Dhruv Batra. Grad-cam: Visual explanations from deep networks via gradient-based localization. In *Proceedings of the IEEE international conference on computer vision*, pages 618–626, 2017. 2, 4
- [70] Rui Shao, Pramuditha Perera, Pong C Yuen, and Vishal M Patel. Open-set adversarial defense. In *Computer Vision—ECCV 2020: 16th European Conference, Glasgow, UK, August 23–28, 2020, Proceedings, Part XVII 16*, pages 682–698. Springer, 2020. 1
- [71] Abhishek Sinha, Kumar Ayush, Jiaming Song, Burak Uzsent, Hongxia Jin, and Stefano Ermon. Negative data augmentation. In *International Conference on Learning Representations*, 2021. 4
- [72] Kihyuk Sohn, Chun-Liang Li, Jinsung Yoon, Minho Jin, and Tomas Pfister. Learning and evaluating representations for deep one-class classification. *arXiv preprint arXiv:2011.02578*, 2020. 4
- [73] Luc PJ Sträter, Mohammadreza Salehi, Efstratios Gavves, Cees GM Snoek, and Yuki M Asano. Generalad: Anomaly detection across domains by attending to distorted features. *arXiv preprint arXiv:2407.12427*, 2024. 1, 2, 3, 4
- [74] Christian Szegedy, Wojciech Zaremba, Ilya Sutskever, Joan Bruna, Dumitru Erhan, Ian Goodfellow, and Rob Fergus. Intriguing properties of neural networks. *arXiv preprint arXiv:1312.6199*, 2013. 1
- [75] Jihoon Tack, Sangwoo Mo, Jongheon Jeong, and Jinwoo Shin. Csi: Novelty detection via contrastive learning on distributionally shifted instances. *Advances in neural information processing systems*, 33:11839–11852, 2020. 1, 4
- [76] Jeremy Tan, Benjamin Hou, James Batten, Huaqi Qiu, and Bernhard Kainz. Detecting outliers with foreign patch interpolation. *Machine Learning for Biomedical Imaging*, 1(April 2022):1–27, 2022. 8
- [77] Maximilian E Tschuchnig and Michael Gadermayr. Anomaly detection in medical imaging—a mini review. In *Data Science—Analytics and Applications: Proceedings of the 4th International Data Science Conference—iDSC2021*, pages 33–38. Springer, 2022. 1
- [78] Qi Wang, Junyu Gao, and Xuelong Li. Weakly supervised adversarial domain adaptation for semantic segmentation in urban scenes. *IEEE Transactions on Image Processing*, 28(9):4376–4386, 2019. 2
- [79] Weiping Wang, Zhaorong Wang, Zhanfan Zhou, Haixia Deng, Weiliang Zhao, Chunyang Wang, and Yongzhen Guo. Anomaly detection of industrial control systems based on transfer learning. *Tsinghua Science and Technology*, 26(6): 821–832, 2021. 1

- [80] Yue Xing, Qifan Song, and Guang Cheng. Why do artificially generated data help adversarial robustness. *Advances in Neural Information Processing Systems*, 35:954–966, 2022. [2](#)
- [81] Han Xu, Yao Ma, Haochen Liu, Debayan Deb, Hui Liu, Jiliang Tang, and Anil K. Jain. Adversarial attacks and defenses in images, graphs and text: A review, 2019. [3](#)
- [82] Jingkang Yang, Kaiyang Zhou, Yixuan Li, and Ziwei Liu. Generalized out-of-distribution detection: A survey. *International Journal of Computer Vision*, pages 1–28, 2024. [1](#)
- [83] Hang Yao, Ming Liu, Haolin Wang, Zhicun Yin, Zifei Yan, Xiaopeng Hong, and Wangmeng Zuo. Glad: Towards better reconstruction with global and local adaptive diffusion models for unsupervised anomaly detection. *arXiv preprint arXiv:2406.07487*, 2024. [1](#), [3](#)
- [84] Zhiyuan You, Lei Cui, Yujun Shen, Kai Yang, Xin Lu, Yu Zheng, and Xinyi Le. A unified model for multi-class anomaly detection. *Advances in Neural Information Processing Systems*, 35:4571–4584, 2022. [3](#)
- [85] Xiaoyong Yuan, Pan He, Qile Zhu, and Xiaolin Li. Adversarial examples: Attacks and defenses for deep learning. *IEEE transactions on neural networks and learning systems*, 30(9): 2805–2824, 2019. [1](#), [3](#)
- [86] Sangdoon Yun, Dongyoon Han, Seong Joon Oh, Sanghyuk Chun, Junsuk Choe, and Youngjoon Yoo. Cutmix: Regularization strategy to train strong classifiers with localizable features, 2019. [4](#)
- [87] Sergey Zagoruyko and Nikos Komodakis. Wide residual networks, 2017. [3](#)
- [88] Manzil Zaheer, Guru Guruganesh, Avinava Dubey, Joshua Ainslie, Chris Alberti, Santiago Ontanon, Philip Pham, Anirudh Ravula, Qifan Wang, Li Yang, and Amr Ahmed. Big bird: Transformers for longer sequences, 2021. [2](#)
- [89] Vitjan Zavrtanik, Matej Kristan, and Danijel Skočaj. Draem-a discriminatively trained reconstruction embedding for surface anomaly detection. In *Proceedings of the IEEE/CVF International Conference on Computer Vision*, pages 8330–8339, 2021. [3](#), [4](#)
- [90] Vitjan Zavrtanik, Matej Kristan, and Danijel Skočaj. Dsr – a dual subspace re-projection network for surface anomaly detection, 2022. [3](#)
- [91] Chaoning Zhang, Philipp Benz, Chenguo Lin, Adil Karjauv, Jing Wu, and In So Kweon. A survey on universal adversarial attack. *arXiv preprint arXiv:2103.01498*, 2021. [1](#)
- [92] Hui Zhang, Zheng Wang, Zuxuan Wu, and Yu-Gang Jiang. Diffusionad: Norm-guided one-step denoising diffusion for anomaly detection. *arXiv preprint arXiv:2303.08730*, 2023. [1](#)
- [93] Lin Zhang and Yang Dai. A gan anomaly detection method based on multi-scale endogenous enhancement. In *Blockchain and Web3 Technology Innovation and Application Exchange Conference*, pages 269–281. Springer, 2024. [2](#)
- [94] Yang Zou, Jongheon Jeong, Latha Pemula, Dongqing Zhang, and Onkar Dabeer. Spot-the-difference self-supervised pre-training for anomaly detection and segmentation. In *European Conference on Computer Vision*, pages 392–408. Springer, 2022. [1](#), [2](#)

PatchGuard: Adversarially Robust Anomaly Detection and Localization through Vision Transformers and Pseudo Anomalies

Supplementary Material

A. Additional Related Work

In this section, we shed more light on some of the previous pioneering works in AD and AL, and their pipeline.

Recontrast [31] innovates anomaly detection through contrastive reconstruction by adapting encoder and decoder networks specifically to the target domain. Unlike traditional approaches relying on frozen pre-trained encoders, it embeds contrastive learning elements into feature reconstruction to stabilize training, avoid pattern collapse, and improve domain relevance. This ensures precise anomaly detection in industrial and medical imaging tasks.

Transformaly [16] focuses on anomaly detection using a dual-feature approach. It leverages a pre-trained ViT to extract agnostic feature vectors and employs teacher-student training to fine-tune a student network on normal samples. This complementary representation enhances anomaly detection, achieving high AUROC results in unimodal and multimodal settings.

GeneralAD [73] utilizes a Vision Transformer-based framework for anomaly detection across diverse domains. It introduces a self-supervised anomaly feature generation module to create pseudo-abnormal samples by applying operations like noise addition and patch shuffling. These are fed into an attention-based discriminator to detect and localize anomalies while producing interpretable anomaly maps.

GLASS [13] uses gradient ascent for anomaly synthesis. This unified approach combines global anomaly synthesis to manipulate feature manifolds and local strategies to refine weak anomalies. Together, it improves the precision and breadth of industrial anomaly detection and localization.

B. Augmentation Details

In this section, we clarify the soft and hard augmentations, $t_i^s, t_i^h, v_i^s, v_i^h$, which are used in the foreground estimation part of our method. Here, we explain in more detail what these augmentations are and what are the rationales behind choosing them.

Soft Augmentations. Soft augmentations refer to transformations that do not alter the semantic content of the image, preserving the original context and interpretability of the visual information. Examples include color jitter (which modifies brightness, contrast, saturation, or hue slightly), color tint (adding a consistent color overlay), grayscale conversion (removing color information but maintaining structure), and minor Gaussian noise (introducing slight variations that mimic sensor noise). These transformations ensure that the

augmented images remain perceptually similar to the originals, focusing on maintaining semantic integrity while introducing subtle variability. Such augmentations are critical in our method for refining the estimation of the foreground without distorting the regions of interest.

Hard Augmentations. Hard augmentations, in contrast, involve transformations that can significantly alter the semantic meaning or structure of the image. Examples include large rotations (which may distort spatial relationships), extreme cropping (removing substantial portions of the image, potentially excluding key objects), elastic transformations (which deform image structures in ways that can obscure original semantics), and heavy noise injection. These transformations challenge the robustness of the foreground estimation by introducing substantial changes, effectively creating conditions where the boundaries of semantic preservation are tested. In our method, hard augmentations are designed to evaluate the resilience of the anomaly generation process and its ability to adapt under challenging conditions.

C. Additional Ablation Studies

C.1. Clean Training

In this section, we chose to omit adversarial training and instead trained our method using standard training while keeping all other components unchanged. The results reveal an improvement in clean performance, highlighting PatchGuard’s effectiveness across various training and evaluation scenarios. These results are detailed in Table 7. Additionally, we evaluated the clean-trained model under an adversarial setup, demonstrating that our pipeline benefits significantly from adversarial training. This underscores the impact of our regularization technique in adversarial training, which enhances the robustness of attention-based mechanisms against adversarial examples.

Table 7. Performance of the model trained without adversarial training under clean and adversarial setups.

Method	Task	Dataset			
		MVTec AD	VisA	BTAD	BraTS2021
Clean	AD	94.7 / 12.9	93.9 / 16.3	91.3 / 11.6	97.1 / 10.7
	AL	97.4 / 12.5	98.0 / 8.1	95.7 / 11.6	98.5 / 12.3

C.2. Ablation on δ

To determine the attention degree for an output token in an attention head, you need to identify how many of the total input tokens it attends to more than the others. In our case, the ViT model has 256 input tokens. Intuitively, we set δ to $\frac{1}{255}$, drawn from a uniform distribution. In Table 8, we present an ablation study on the value of δ .

Table 8. Ablation study on the value of δ and its effect on the attention degree in the ViT model.

δ	Task	Dataset			
		MVTec AD	VisA	BTAD	BraTS2021
$\frac{1}{2 \times 256}$	AD	89.0 / 69.1	88.8 / 72.1	86.7 / 79.4	94.4 / 79.4
	AL	93.1 / 70.9	96.8 / 82.0	94.0 / 70.8	97.8 / 90.1
$\frac{1}{256}$	AD	88.1 / 71.1	88.5 / 74.3	85.3 / 82.1	94.3 / 81.0
	AL	92.7 / 73.8	96.9 / 85.2	93.2 / 73.0	97.7 / 94.5
$\frac{2}{256}$	AD	85.1 / 71.9	84.7 / 75.8	82.4 / 82.8	91.7 / 81.3
	AL	88.6 / 74.3	93.4 / 85.6	90.3 / 74.1	92.7 / 81.9

C.3. Diffenet ViT Backbone

As mentioned in the implementation details, we used a ViT small model with a patch size of 14, initialized with random weights. In this section, we evaluate our method by replacing the backbone with larger variations of ViT models (note that these models use random weights and are not pre-trained). All other components are kept fixed. As shown in Table 9, the results demonstrate that our method achieves high performance and consistency across different backbones.

Table 9. Evaluation of our method with different ViT backbones initialized with random weights. The results demonstrate high performance and consistency across various backbone configurations.

ViT	Task	Dataset			
		MVTec AD	VisA	BTAD	BraTS2021
Small(<i>Ours</i>)	AD	88.1 / 71.1	88.5 / 74.3	85.3 / 82.1	94.3 / 81.0
	AL	92.7 / 73.8	96.9 / 85.2	93.2 / 73.0	97.7 / 94.5
Base	AD	89.1 / 71.0	87.9 / 73.1	84.5 / 81.7	93.0 / 82.3
	AL	91.0 / 72.6	95.8 / 82.1	94.7 / 74.8	98.4 / 94.9
Large	AD	90.0 / 70.6	87.5 / 74.7	85.5 / 81.9	95.1 / 81.6
	AL	92.9 / 73.4	95.8 / 86.0	94.1 / 73.5	96.7 / 93.2

C.4. Backbone

In Sections 4 and 5, we provided intuitions and theoretical insights on why vision transformers achieve better adversarial robustness than convolution-based methods. In this section, we use convolution-based backbones in our pipeline

instead on the ViT, while preserving all other components as they are. To support this claim, we provide the detection and localization results in Table 10.

Adapting convolution-based backbones like ResNet [32] to our patch-based pipeline poses certain challenges. To integrate ResNet, we incorporate a binary classification layer at the model’s final stage. Each image is divided into patches manually, following the same patching approach used by the vision transformer. Anomaly scores are then computed for each patch independently, and the final anomaly detection decision is based on the top- k patches with the highest scores. For a fair comparison, we apply the same hyperparameters used in our original method.

To adapt U-Net [65], we shift from a patch-wise approach to pixel-wise localization, given the architectural constraints of U-Net. Notably, the top- k selection used previously is incompatible in this context. Instead, we employ a top- p percent pixel selection for the anomaly detection decision, where $p = \frac{k}{N}$, and N represents the total number of patches in an image.

C.5. Integrating Sparse Attention Mechanism into Our Methodology

We evaluate the performance of our method after incorporating BigBird [88], a sparse attention mechanism, as shown in Table 11. The results reveal two key findings. First, applying the sparse attention mechanism generally reduces the robustness of our method. This aligns with our intuition and theory, which suggest that a higher attention degree enhances model robustness, while sparse attention decreases the attention degree. Second, our regularization term remains effective even in the sparse attention setup—when applied, it still improves the model’s robustness.

C.6. Impact of Regularization Layer on Model Performance

We investigated the effect of applying regularization to different layers of the network. The results, shown in Table 12, indicate that regularization in inner layers generally improves model robustness. However, the last layer performs slightly better according to our experiments.

Table 10. A study on the performance of various backbone networks, as alternatives to the ViT, within our architecture.

Backbone	Task	Dataset			
		MVTec-AD	VisA	BTAD	BraTS2021
U-Net	AD	84.7 / 15.1	80.0 / 15.7	76.9 / 14.0	70.3 / 12.9
	AL	85.4 / 17.8	81.8 / 13.9	79.6 / 18.2	76.3 / 16.0
Resnet50	AD	88.1 / 27.6	84.9 / 23.3	85.7 / 23.9	86.0 / 23.5
	AL	87.1 / 28.3	83.7 / 24.6	86.0 / 24.7	85.1 / 23.9

Table 11. Performance comparison of our method with and without the BigBird sparse attention mechanism.

Backbone	Task	MVTec AD	VisA	BTAD	BraTS2021
BigBird	AD	86.7 / 51.7	90.3 / 49.7	86.0 / 58.9	95.9 / 61.8
	AL	91.4 / 53.1	93.9 / 59.8	92.5 / 51.4	96.4 / 68.5
BigBird + Our Regularization	AD	85.6 / 63.0	88.5 / 61.4	86.2 / 69.8	92.2 / 73.1
	AL	90.0 / 64.7	92.1 / 73.6	90.5 / 62.2	94.6 / 78.9
Ours	AD	88.1 / 71.1	88.5 / 74.3	85.3 / 82.1	94.3 / 81.0
	AL	92.7 / 73.8	96.9 / 85.2	93.2 / 73.0	97.7 / 94.5

Table 12. Performance of Regularization at Different Layers

Regularization Layer	Task	MVTec AD	VisA	BTAD	BraTS2021
$(N - 2)^{\text{th}}$	AD	87.3 / 68.2	89.7 / 72.9	86.3 / 79.1	93.5 / 75.4
	AL	91.5 / 70.6	96.0 / 83.1	91.7 / 68.5	96.8 / 90.6
$(N - 1)^{\text{th}}$	AD	89.0 / 69.4	87.5 / 73.1	84.3 / 82.3	92.6 / 79.9
	AL	93.2 / 70.6	95.7 / 86.1	93.1 / 71.7	97.0 / 93.2
N^{th} (Last Layer)	AD	88.1 / 71.1	88.5 / 74.3	85.3 / 82.1	94.3 / 81.0
	AL	92.7 / 73.8	96.9 / 85.2	93.2 / 73.0	97.7 / 94.5

D. Dataset Details

We conducted our experiments on eight datasets covering a diverse range of domains, from industrial to medical applications. The medical datasets include BraTS2021 and Head-CT, while the remaining six datasets focus on industrial and synthetic anomaly detection and localization tasks. Below, we provide detailed descriptions of each dataset.

- **MVTec AD:** MVTEC AD is a dataset for benchmarking anomaly detection methods in industrial inspection. It includes over 5,000 high-resolution images across fifteen object and texture categories. Each category contains defect-free training images and a test set with both normal and defective samples, featuring defects like scratches, dents, and misalignments.
- **VisA:** The VisA dataset contains 12 object subsets with 10,821 images, comprising 9,621 normal samples and 1,200 anomalous samples. The subsets include printed circuit boards, multi-instance objects like Capsules and Macaroni, and roughly aligned objects such as Cashew and Chewing Gum. Anomalies include surface defects like scratches and dents, and structural issues such as missing components.
- **BTAD:** The BTAD [61] consists of 2,830 images of three industrial products. It provides samples with body and surface defects, intended for evaluating visual anomaly detection methods in industrial settings.
- **MPDD:** MPDD [40] is a dataset for defect detection in metal parts manufacturing, consisting of over 1,000 images with pixel-level defect annotations. The dataset is divided into six distinct classes and includes anomaly-free training samples and test samples with normal and defective parts, covering a variety of surface and structural defects.
- **WFDD:** WFDD [13] is a dataset for anomaly detection in textile inspection, comprising 4,101 woven fabric images

across four categories: grey cloth, grid cloth, yellow cloth, and pink flower. Defects are categorized as block-shaped, point-like, or line-type, with pixel-level annotations.

- **DTD-Synthetic:** The DTD-Synthetic [3] is designed for anomaly detection and segmentation tasks, containing synthetic texture images generated from predefined texture patterns. It includes twelve classes of normal texture samples and those with artificially introduced anomalies such as structural distortions or irregular patterns.
- **BraTS2021:** BraTS2021 is a medical dataset for anomaly segmentation, containing 1,251 MRI cases with voxel-level annotations for tumor regions. Each case includes multiple imaging modalities (T1, T1ce, T2, and FLAIR). In this paper, only the FLAIR modality is used due to its sensitivity to tumor regions.
- **Head-CT:** The Head-CT [42] contains 200 head CT slices, evenly split between normal slices and those with hemorrhages, without distinguishing between hemorrhage types.

E. Details of Adaptation of State-of-the-Art Methods for Adversarial Robustness

Before proposing a novel approach for adversarial AD and AL setups, our idea was to adapt existing state-of-the-art methods in the field and enhance their robustness through adversarial training [13, 31, 73, 83]. Adversarial training involves feeding adversarial examples to the model during training [54]. In the following section, we explain how we create adversarial examples for each method and the details of our best approach to make them robust, which are reported in Table 3.

Anomaly-free methods like PatchCore [66] and ReContrast [31] have anomaly-free training. For adapting PatchCore, we used an adversarially trained ResNet-50 [32] as the feature extractor. Adding adversarially generated normal samples to the memory bank was tested but did not improve performance. For adapting ReContrast, we replaced both the teacher and student networks with adversarially trained ResNet-50 models, and using adversarial samples generated by the PGD-100 attack [54] on the final anomaly map, we trained the network to improve robustness.

Embedding-space synthesis methods, such as GeneralAD [73] and SimpleNet [49], operate in the embedding space. For adapting SimpleNet, we employed an adversarially robust WideResNet-50 [87] as the feature extractor. Two strategies were tested: input-space adversarial training, which was ineffective due to the absence of anomaly samples, and embedding-space adversarial training, where the discriminator was adversarially trained using both normal and anomaly features. The latter approach performed better, as reported in Table 3, but the overall performance was still insufficient. For GeneralAD, due to the model’s dependency on DINO [9] pre-trained weights, we could not find a proper robust pre-trained ViT backbone for adaptation that maintained

Table 13. Class-wise Clean and Adversarial AUROC (%) Results for Image-level and Pixel-level Evaluations on the MVTEC-AD Dataset.

Class Name	Image-level AUROC (%)		Pixel-level AUROC (%)	
	Clean	Adversarial	Clean	Adversarial
Bottle	97.6	84.7	96.7	84.6
Cable	87.3	74.0	97.2	77.8
Capsule	71.8	79.6	93.6	85.2
Carpet	83.9	43.2	95.8	53.7
Grid	95.7	74.9	93.1	55.5
Hazelnut	99.5	80.5	97.2	91.3
Leather	91.0	80.2	97.6	67.6
Metal Nut	88.8	54.4	87.9	75.3
Pill	81.5	59.1	86.7	76.3
Screw	55.4	56.6	93.8	86.5
Tile	95.3	71.7	86.2	64.0
Toothbrush	100	90.6	93.9	81.9
Transistor	94.1	84.3	95.4	84.8
Wood	93.1	56.0	89.6	57.4
Zipper	87.6	76.9	86.2	65.7

clean performance. We tested multiple approaches to make it robust while maintaining clean performance, and the best one was embedding-space adversarial training of the discriminator with access to both normal and anomaly features, and replacing the ViT with a robust pre-trained model on ImageNet [19].

Input-space synthesis methods like DRAEM [89] and GLASS [13] generate synthetic anomalies in the input space. In adapting DRAEM, adversarial samples were created using PGD-100 on the focal loss [46] of the anomaly map, and these samples were used to train both the reconstructive and discriminative sub-networks adversarially. For adapting GLASS, the best results were achieved by combining an adversarially trained feature extractor with adversarial samples (PGD-100) applied to both L_n and L_{las} .

According to Table 3, state-of-the-art methods in AD and AL, even after adapting to adversarial training scenarios, still suffer from vulnerability to adversarial attacks and perform weakly.

F. Per-Class Results

In this section, we present the per-class AUROC results for anomaly detection and localization using PatchGuard across the reported datasets, as detailed in Tables 13, 14, 15, 16, 17, and 18.

G. Implementation Details

The optimizer used is AdamW [51], with a learning rate of 0.0008 and a weight decay of 0.00001. For learning rate scheduling, we utilize a CosineAnnealingLR scheduler with a decay factor of 0.0125, where the minimum learning

Table 14. Class-wise Clean and Adversarial AUROC (%) Results for Image-level and Pixel-level Evaluations on the VisA Dataset.

Class Name	Image-level AUROC (%)		Pixel-level AUROC (%)	
	Clean	Adversarial	Clean	Adversarial
Candle	83.6	82.5	94.9	70.7
Capsules	77.7	66.2	97.1	57.0
Cashew	88.7	83	97.3	89.9
Chewing gum	92.2	73.5	97.7	92.2
Fryum	85.1	74.5	95.9	88.0
Macaroni 1	86.5	66.2	97.0	84.8
Macaroni 2	68.3	42.3	95.3	85.0
Pcb 1	95.4	85.3	99.0	95.4
Pcb 2	97.3	91.2	96.8	87.1
Pcb 3	94.8	73.5	98.7	93.0
Pcb 4	98.5	92.1	95.9	83.7
Pipe fryum	94.3	61.5	98.1	96.2

Table 15. Class-wise Clean and Adversarial AUROC (%) Results for Image-level and Pixel-level Evaluations on the BTAD Dataset.

Class Name	Image-level AUROC (%)		Pixel-level AUROC (%)	
	Clean	Adversarial	Clean	Adversarial
01	98.6	96.1	91.7	77.1
02	65.3	65.6	92.1	64.2
03	92.0	84.6	95.8	77.8

Table 16. Class-wise Clean and Adversarial AUROC (%) Results for Image-level and Pixel-level Evaluations on the MPDD Dataset.

Class Name	Image-level AUROC (%)		Pixel-level AUROC (%)	
	Clean	Adversarial	Clean	Adversarial
Bracket Black	83.4	60.1	92.1	88.4
Bracket Brown	84.5	77.4	91.0	84.7
Bracket White	79.8	52.9	92.1	85.9
Connector	94.3	92.5	93.8	76.8
Metal Plate	100	86.2	98.2	95.2
Tubes	70.4	42.8	95.9	88.9

Table 17. Class-wise Clean and Adversarial AUROC (%) Results for Image-level and Pixel-level Evaluations on the WFDD Dataset.

Class Name	Image-level AUROC (%)		Pixel-level AUROC (%)	
	Clean	Adversarial	Clean	Adversarial
Gray Cloth	88.8	57.3	93.1	75.9
Grid Cloth	99.6	94.7	97.8	85.1
Pink Flower	52.3	33.0	94.4	63.0
Yellow Cloth	96.3	75.0	93.3	62.5

rate (η_{\min}) is calculated as $\text{lr} \times \text{lr_decay_factor}$, and T_{\max} is set to the number of epochs, which is set to 300 but we observe empirically that convergence usually happens much faster. The batch size for both training and testing is set to 16. The input image size is 224×224 . We use a ViT

Table 18. Class-wise Clean and Adversarial AUROC (%) Results for Image-level and Pixel-level Evaluations on the DTD-Synthetic Dataset.

Class Name	Image-level AUROC (%)		Pixel-level AUROC (%)	
	Clean	Adversarial	Clean	Adversarial
	Blotchy 099	86.1	73.2	94.7
Fibrous 183	100	55.8	99.0	80.9
Marbled 078	89.3	63.8	97.6	88.4
Matted 069	93.1	53.8	97.1	78.1
Mesh 114	94.4	74.9	97.6	73.6
Perforated 037	99.9	81.1	94.4	55.5
Stratified 154	91.6	42.5	98.2	76.2
Woven 001	83.6	56.0	96.2	71.6
Woven 068	88.5	55.5	93.6	71.4
Woven 104	79.6	55.4	87.9	73.0
Woven 125	95.3	56.9	98.2	71.6
Woven 127	96.8	57.9	97.2	70.5

(Vision Transformer) small model as the feature extractor, which is not pre-trained. Finally, we perform a top- k selection of the localization map achieved, to obtain a final AD decision, with k being set to 5.

H. Attack Adaptation Details

Adaptation Classification Attack. We evaluated PatchGuard’s resilience against several advanced adapted attacks from the classification domain, including CAA, AutoAttack, A3, and PGD-1000. Originally designed to compromise classification tasks by exploiting the cross-entropy loss, these attacks were adapted for anomaly localization (AL) and anomaly detection (AD) tasks. The focus was on altering the sum of cross-entropy for all patches in detector models, aiming to increase the loss values for normal regions of test samples while decreasing them for anomalous regions. Adapting AutoAttack (AA) for AD and AL tasks posed significant challenges. AutoAttack comprises a suite of different attack methods, such as FAB, multi-targeted FAB, Square Attack, APGDT, APGD with cross-entropy loss, and APGD with DLR loss. The primary difficulty in adaptation arises because attacks using the DLR loss assume the model’s output contains at least three elements, an assumption valid for classification tasks with three or more classes but not applicable to AD and AL tasks. Consequently, we replaced the DLR loss component in AutoAttack with a PGD attack. However, for the other attacks under consideration, no modifications were necessary.

Adaptation Segmentation Attack. We evaluate our method against advanced adapted semantic segmentation attacks, specifically SegPGD and SEA, with a key modification: instead of operating at the pixel level, our approach applies these attacks patch-wise. SegPGD is a segmentation-specific adaptation of the Projected Gradient Descent (PGD) attack that dynamically balances focus between misclassi-

Table 19. Comparison of our model’s performance with and without the attention discriminator.

Method	Task	Dataset			
		MVTec AD	VisA	BTAD	BraTS2021
w/o discriminator	AD	85.9 / 69.5	87.7 / 73.0	83.8 / 80.6	93.4 / 80.6
	AL	91.1 / 71.5	95.4 / 83.9	91.7 / 72.2	96.4 / 93.5
w/ discriminator (<i>Ours</i>)	AD	88.1 / 71.1	88.5 / 74.3	85.3 / 82.1	94.3 / 81.0
	AL	92.7 / 73.8	96.9 / 85.2	93.2 / 73.0	97.7 / 94.5

fied and correctly classified pixels. It starts by prioritizing correctly classified pixels, progressively shifting its emphasis to achieve an effective balance as the attack unfolds. On the other hand, SEA integrates multiple complementary loss functions, such as Jensen-Shannon divergence and Masked Cross-Entropy, to exploit various weaknesses in model robustness. Through progressive radius reduction and adaptive optimization, SEA generates potent adversarial perturbations, selecting the worst-case attack outcome to ensure a thorough robustness evaluation.

I. Attention Discriminator

The attention discriminator in our method plays a pivotal role in the anomaly detection and localization pipeline. Conceptually, this component operates similarly to a single layer of a Vision Transformer, where the input embeddings undergo self-attention operations. The resulting embeddings are subsequently passed through a Multi-Layer Perceptron (MLP) to compute a set of anomaly scores for each embedding. Furthermore, the “Attention Degrees,” introduced in previous sections, are derived directly from this attention discriminator, reinforcing its critical position in our framework.

To substantiate the necessity and efficacy of the attention discriminator, we performed an ablation study, the results of which are presented in Table 19. In the alternative setup without the discriminator, the attention degrees and MLP components are instead placed on top of the ViT’s final layer. This bypass eliminates the intermediate role played by the attention discriminator. However, the comparative results demonstrate that the inclusion of the attention discriminator provides marginally superior performance. This advantage highlights its significance not only in enhancing the model’s performance but also in improving its interpretability by providing more precise and structured attention degree calculations.

J. Evaluating Our Model Under Various Attacks with Diverse Epsilon

To demonstrate our model’s robustness, we conducted an experiment in which we trained it under varying ϵ values of PGD with l_∞ norm and evaluated it using the same ϵ (ensur-

ing that the training and evaluation ϵ were identical). The results, as presented in Table 20, indicate that PatchGuard performs effectively across different ϵ values.

Table 20. Performance of PatchGuard under varying ϵ values, demonstrating consistent robustness and effectiveness across different settings.

Epsilon	Task	Dataset			
		MVTec AD	VisA	BTAD	BraTS2021
$\frac{2}{255}$	AD	90.1 / 80.3	89.6 / 77.8	88.3 / 85.6	95.7 / 86.3
	AL	94.0 / 81.6	97.1 / 88.7	93.7 / 79.1	98.2 / 95.3
$\frac{4}{255}$	AD	88.9 / 74.2	88.8 / 75.4	86.0 / 83.5	94.8 / 83.4
	AL	93.2 / 76.4	97.1 / 77.5	93.1 / 75.4	97.9 / 94.6
$\frac{8}{255}$ (<i>Ours</i>)	AD	88.1 / 71.1	88.5 / 74.3	85.3 / 82.1	94.3 / 81.0
	AL	92.7 / 73.8	96.9 / 85.2	93.2 / 73.0	97.7 / 94.5

In this section, we evaluate PatchGuard trained on PGD-10 with l_∞ norm under $\epsilon = \frac{8}{255}$ using PGD-1000 with l_2 norms with various ϵ . As shown in Table 20, our model remains robust against these types of attacks.

Table 21. Evaluation of PatchGuard’s robustness when trained on PGD-10 with l_∞ norm under $\epsilon = \frac{8}{255}$, assessed using PGD-1000 with l_2 norms with various ϵ . The results demonstrate the model’s sustained robustness against different types of attacks.

ϵ	Task	Dataset			
		MVTec AD	VisA	BTAD	BraTS2021
Clean	AD	88.1	88.5	85.3	94.3
	AL	92.7	96.9	93.2	97.7
$\frac{16}{255}$	AD	84.3	82.7	81.7	89.2
	AL	85.7	91.7	84.3	96.7
$\frac{32}{255}$	AD	82.1	81.0	79.5	87.4
	AL	83.6	90.3	82.9	96.1
$\frac{64}{255}$	AD	78.2	79.8	78.5	86.4
	AL	81.0	88.7	79.6	95.7
$\frac{128}{255}$	AD	77.2	78.6	76.7	84.7
	AL	78.3	86.7	77.9	95.0

K. Limitations

Our proposed PatchGuard method includes a “foreground-aware anomaly generation” component that leverages Grad-CAM, which inherently ties our approach to a pretrained model. While this dependency enables our method to focus on relevant regions, it also introduces reliance on the quality

and biases of the pretrained model. Furthermore, although we employ soft augmentations to encourage this component to identify accurate regions, there is no theoretical guarantee that it consistently achieves this objective. Nonetheless, as our empirical results demonstrate, the component performs well in practice, effectively highlighting anomalies in diverse scenarios.

L. Trade-Off Between Anomaly Detection and Localization

The anomaly score and localization map of a method play a crucial role in shaping the design of attacks, enabling attackers to target either anomaly localization or detection with greater precision. In this study, however, we design our attacks on other methods to simultaneously target both localization and detection. In our proposed method, PatchGuard, the anomaly score is derived as the average of the top-k values in the anomaly map. This mechanism ensures that the optimal attack strategy for anomaly detection inherently aligns with the strategy for anomaly localization.

A particularly noteworthy aspect of our study is the approach we use to attack anomaly localization. Specifically, we flip anomaly patches to appear normal and normal patches to appear anomalous. An alternative logical attack could involve manipulating normal images to make all pixels anomalous, while for anomalous samples, the attack would preserve the normal pixels as they are and convert the anomalous pixels to appear normal. This approach would ultimately make the anomaly map of an anomalous sample indistinguishable from that of a normal sample.

Although this alternative attack is specifically designed for anomaly detection, it is far less effective for anomaly localization. Existing methods, even without explicitly addressing this type of targeted attack, are already highly vulnerable to detection-based attacks. In contrast, our method has been experimentally shown to be robust against such attacks. This robustness arises from our use of stronger adversarial training strategies, where all pixels are flipped to create more challenging adversarial examples during the training process.

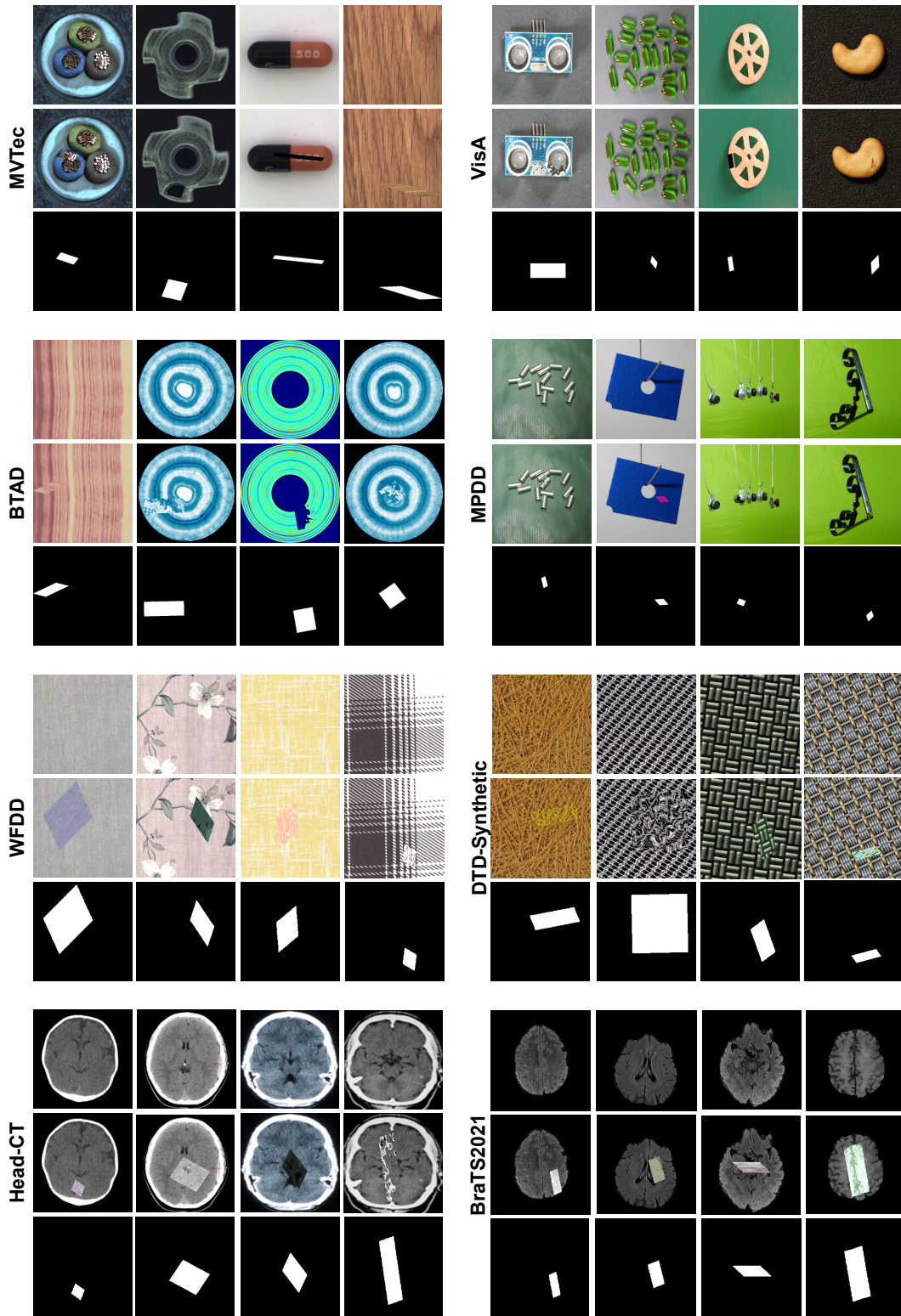


Figure 4. Visualization of Pseudo-Anomaly Generated for Each Dataset. Each group corresponds to one dataset: MVTEc AD, VisA, BTAD, MPDD, WFDD, DTD-Synthetic, BraTS2021, and Head-CT. Within each group, columns represent randomly selected samples from the respective dataset. The first row shows a normal image, the second row depicts the corresponding pseudo-anomaly generated image, and the third row illustrates the associated anomaly mask.